Benzotriazole Adsorption on $Cu_2O(111)$ Surfaces: A First-Principles Study

Yong Jiang,*,† James B. Adams,†,‡ and Donghai Sun‡

Science and Engineering of Materials Program, Arizona State University, Tempe, Arizona 85287-1704, and Department of Chemical and Materials Engineering, Arizona State University, Tempe, Arizona 85287-6006

Received: February 5, 2004; In Final Form: June 26, 2004

The adsorption of benzotriazole (BTAH) on $Cu_2O(111)$ was investigated with use of first-principles density functional theory calculations. Two possible adsorption structures were considered for both one-quarter and full adsorption coverage. We found that BTAH strongly chemisorbs (1.2−1.5 eV) onto $Cu_2O(111)$ by forming a chemical bond with a surface copper atom through nitrogen sp^2 lone pairs, and a hydrogen bond with a surface oxygen atom through a C−H or N−H proton. The chemical interaction between the surface copper site and the molecule is the combined effect of a strong lone-pair → hybrid Cu-$d_{z^2}sp_z$ σ-donation and a relatively weak $d_{yz} \rightarrow 6\pi^*$ back-donation. Vibration calculations were carried out to predict the BTAH−Cu_2O stretching frequencies for both adsorption structures. The calculated stretching frequency (381 and 428 cm^{-1}) could overlap with the BTAH benzene-ring torsion band. An estimate for the BTAH−Cu vibrational frequency (226 and 223.4 cm^{-1} for two adsorption modes, respectively) is in good agreement with an experimentally observed Raman peak of 240 cm^{-1}.

1. Introduction

Chemical-mechanical polishing (CMP) of copper is a critical process to pattern copper interconnections and achieve wafer-level global planarization for sub-0.13 um ULSI technologies.[1−3] Benzotriazole (BTAH or $C_6N_3H_5$) is a well-known corrosion inhibitor for Cu since 1947,[4] and has been introduced into Cu−CMP slurries, where it has proven to be able to dramatically reduce undesirable isotropic etching at various pH values without significant reduction of the removal rate.[5−10] The ability of BTAH to inhibit isotropic etching is attributed to the formation of an insoluble Cu(I)BTA polymeric layer that may act as a physical barrier to ionic movement around the surface, thus imparting some degree of corrosion resistance to copper surfaces.[11,12] In our previous work,[13] we used the plane-wave density functional theory (DFT) code VASP to calculate the adsorption structures, binding energies, and intermolecular hydrogen bonds of BTAH molecules on Cu(111).

To increase removal rate, Cu−CMP slurries normally contain oxidants to accelerate the formation of Cu ions. Due to the fact that the thermodynamic stability region of CuBTA overlaps with most of the Cu_2O region in a wide pH range on the Pourbaix diagram,[14] and that BTAH is more often found bound to copper oxides,[15,16] we propose to investigate the adsorption of BTAH on copper oxides. A previous X-ray diffraction study on the aqueous oxidation of Cu(111)[17] has found the oxide on the Cu-(111) surface is crystalline Cu_2O with both aligned and reversed $Cu_2O(111)[110]//Cu(111)[110]$ epitaxial relations being possible. In this study, $Cu_2O(111)$ is assumed on the Cu(111) substrate. The same first-principles approach as our previous work[13] is used to investigate the adsorption of the very first layer of BTAH on $Cu_2O(111)$.

2. Methodology

All relaxation and total energy calculations have been performed by using the plane-wave based Vienna ab initio simulation package (VASP).[18] The exchange-correlation functional was the generalized gradient approximation (GGA) of Perdew and Wang (PW91).[19] Sampling of the irreducible wedge of the Brillouin zone was performed with a Gamma-centered or Monkhorst-Pack grid of special points. Ground-state atomic geometries of single molecules and surfaces were obtained by minimizing the Hellman−Feyman forces using a conjugate gradient algorithm, until the total force on each ion was converged to 0.05 eV/Å. The binding energies were obtained by following the convergence procedure recommended by Kresse.[20] The same computational methodology has been described in more detail in our previous paper.[13] Another code ADF (Amsterdam Density Functional)[21] was employed to perform charge analysis for an isolated BTAH molecule with the PW91 exchange-correlation functional.

TABLE 1: Calculated Bulk Properties of Cu_2O

method	α (Å)	Δ (%)	Bo (GPa)	Δ (%)
LDA-US	4.191	−1.78	146.85	29.95
LDA-PAW	4.179	−2.06	145.93	30.29
GGA-US	4.318	1.19	109.89	−1.88
GGA-PAW	4.310	1.00	106.44	−4.96
HF[23]	4.435	3.94	100.0	−10.71
HF + LYP[23]	4.277	0.23	93	−16.96
EXP	4.267[22]		112[24]	
			114[25]	

3. $Cu_2O(111)$ Surface and BTAH Molecule Calculations

We first validated our methodology by calculating the lattice constant and bulk modulus of Cu_2O by fitting energy vs volume data to the Murnaghan equation of state. Both the ultra-soft (US) and projected augmented wave (PAW) pseudopotentials are generated with valence configurations of Cu-$3d^{10}4p^1$ and O-$2s^2$-$2p^4$, which should be valid for the case of Cu exposed to highly electronegative species such as N. The calculations were performed with an 8 × 8 × 8 Monkhoprst−Pack k-point grid and a 400-eV plane-wave cutoff energy. Table 1 lists the calculated properties of Cu_2O. Calculations with the GGA-US yield results closer to experimental data than other methods,

* Corresponding author. Phone/fax: + 1-9658509. E-mail: yjiang@asu.edu.

† Science and Engineering of Materials Program.

‡ Department of Chemical and Materials Engineering.

10.1021/jp049457b CCC: $27.50
Published on Web 08/04/2004

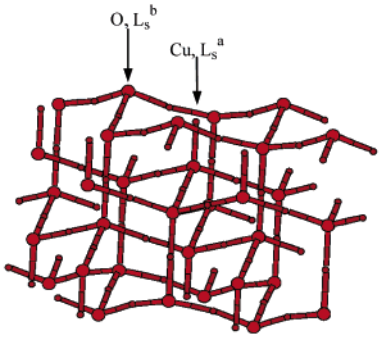

# of layers	9 L	12 L	18 L	24L
Surface Energy γ (J/m^2)	0.751	0.735	0.736	0.736
$\Delta\gamma$ %	-2.077	0.122	0.041	

Figure 1. A relaxed 2 × 2 12-layer $Cu_2O(111)$ (small balls, Cu; larger balls, O) and surface energy convergence w.r.t. the number of layeres.

and therefore it is chosen for the $Cu_2O(111)$ surface calculations. The GGA-US predicted Cu−O bond length in the bulk is 1.870 Å, which is close to the experimental value of 1.845 Å.[22]

Figure 1 shows an ideal $Cu_2O(111)$ surface that is nonpolar and consists of a three-plane repeat unit with each copper layer sandwiched between two layers of oxygen anions.[26] The Cu_2O-(111) unit cell possesses hexagonal symmetry with a Lewis acid site (L_s^a) at unsaturated Cu and a Lewis base site (L_s^b) at unsaturated O. Two $Cu_2O(111)$ substrates of different supercell sizes are constructed to simulate the oxide surface with periodic boundary conditions. The larger substrate is a 2 × 2 hexagonal supercell (a = 12.19 Å, α = 120°, and $\beta = \gamma$ = 90°) used to calculate low-coverage adsorption (0.25 ML). The smaller 2 × 1 orthorhombic supercell (a = 6.095 Å and b = 10.556 Å) is used to calculate saturation adsorption. A vacuum height of at least 10 Å separates the successive slabs and the adsorbed molecules along the z-direction. The $Cu_2O(111)$ surface energy is calculated by slab thickness convergence beginning with 9-layers, until the difference in surface energy between consecutive steps is under 0.5% (see Figure 1). The calculated surface energy is 0.736 J/m^2, but we lack any experimental data to compare with this result. The very small surface relaxations are mainly found in the top two layers, where the O(L_s^b)−Cu bond length shrinks slightly from 1.870 Å to 1.839 Å, while the Cu-(L_s^a)−O length increases to ∼1.902 Å. The main result of the relaxation is a more compact surface where top-layer oxygen anions sink in and copper cations become more exposed. The negligible relaxation as a whole is consistent with the nonpolar character of the surface.

In our previous study of BTAH/Cu(111) adsorption,[13] we obtained the ground-state structure of an isolated BTAH molecule by atomic relaxation using two different cell sizes. The calculated total energies differed by ∼0.11 eV. This difference is not negligible compared with the binding energy (∼0.43 eV), which requires the recalculation of the total energy E(BTAH) for our BTAH/$Cu_2O(111)$ case in the two new supercells. The influence of the cell size and shape on the BTAH structure is so negligible that all bond lengths obtained in our previous study are still valid. Atomic charges of BTAH were calculated by using three methods in the ADF software; they are compared in Figure 2. Mulliken population analysis produces negative charges for C−H protons, which is physically unreasonable. Only Voronoi[27,28] and Hirshfeld[29−31] charges are quantitatively comparable and can give reliable predictions for BTAH (ADF Users' guide recommends Hirshfeld analysis).

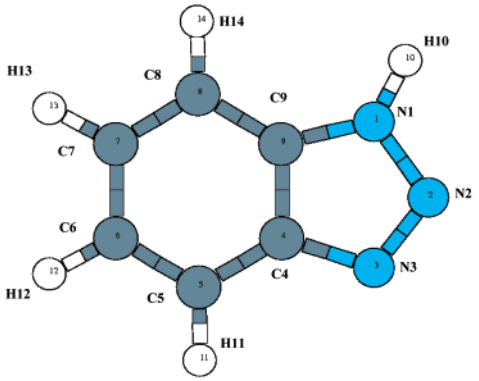

No.	Atom	Charge Flow (e)		
		Mulliken	Voronoi	Hirshfeld
1	N	-0.201	-0.058	-0.034
2	N	-0.111	-0.060	-0.062
3	N	-0.304	-0.127	-0.125
4	C	0.168	-0.002	0.007
5	C	0.040	-0.056	-0.034
6	C	0.011	-0.059	-0.048
7	C	0.023	-0.048	-0.040
8	C	0.009	-0.076	-0.052
9	C	0.249	0.017	0.027
10	H	0.113	0.196	0.157
11	H	0.018	0.085	0.057
12	H	-0.004	0.061	0.048
13	H	-0.001	0.060	0.049
14	H	-0.010	0.068	0.050

Figure 2. BTAH molecule structure and charge distribution.

Hirshfeld analysis shows the strong electron attractive power of the triazole moiety, which reduces the electron density on the benzene ring and NH proton, and consequently C_4, C_9, and all protons become more positive. This results in a large dipole moment of 3.95 D. It is obvious that during adsorption onto $Cu_2O(111)$, the sp^2 lone pairs of the triazole moiety can solely interact with suitable Cu(I) empty orbitals, and protons (especially the N−H proton) can interact with surface oxygen anions via Coulombic forces.

4. BTAH Adsorption on $Cu_2O(111)$

4.1. Adsorption Geometry and Energy. On the basis of our previous calculations on the gas-phase BTAH[13] and bulk Cu_2O, we choose the GGA-US pseudopotential for the Cu_2O surface and GGA-PAW for the BTAH molecules. All the adsorption calculations have been run on a 9-layer Cu_2O surface with the bottom two layers being fixed. Lewis acid−base site pairs on $Cu_2O(111)$ surfaces can facilitate BTAH adsorption. The charge analysis of a single BTAH molecule suggests the adsorption could consist of two processes: the initial formation of a chemical bond through nitrogen lone pairs interacting with a surface copper cation (L_s^a), followed by a hydrogen bond stabilization between a BTAH proton and a surface oxygen anion (L_s^b), or vice versa.[32] On the basis of this scheme, two different orientations of BTAH have been considered on $Cu_2O(111)$: (1) Mid_N mode, N_2−Cu(L_s^a) with a possible (N−)H···O(L_s^b) hydrogen bond, and (2) Side_N mode, N_3−Cu(L_s^a) with a possible (C−)H···O(L_s^b) hydrogen bond. We relaxed the geometry for both modes with a 2 × 2 × 1 Gamma-centered k-point grid and a 400-eV cutoff energy. All the relaxation calculations are performed under the exact same calculation conditions as on the $Cu_2O(111)$ surface, so we can compare one to another to deduce the adsorption energy, ΔE.

$$\Delta E = E(\mathrm{BTAH/Cu_2O}) - E(\mathrm{BTAH}) + E(\mathrm{Cu_2O}) \quad (1)$$

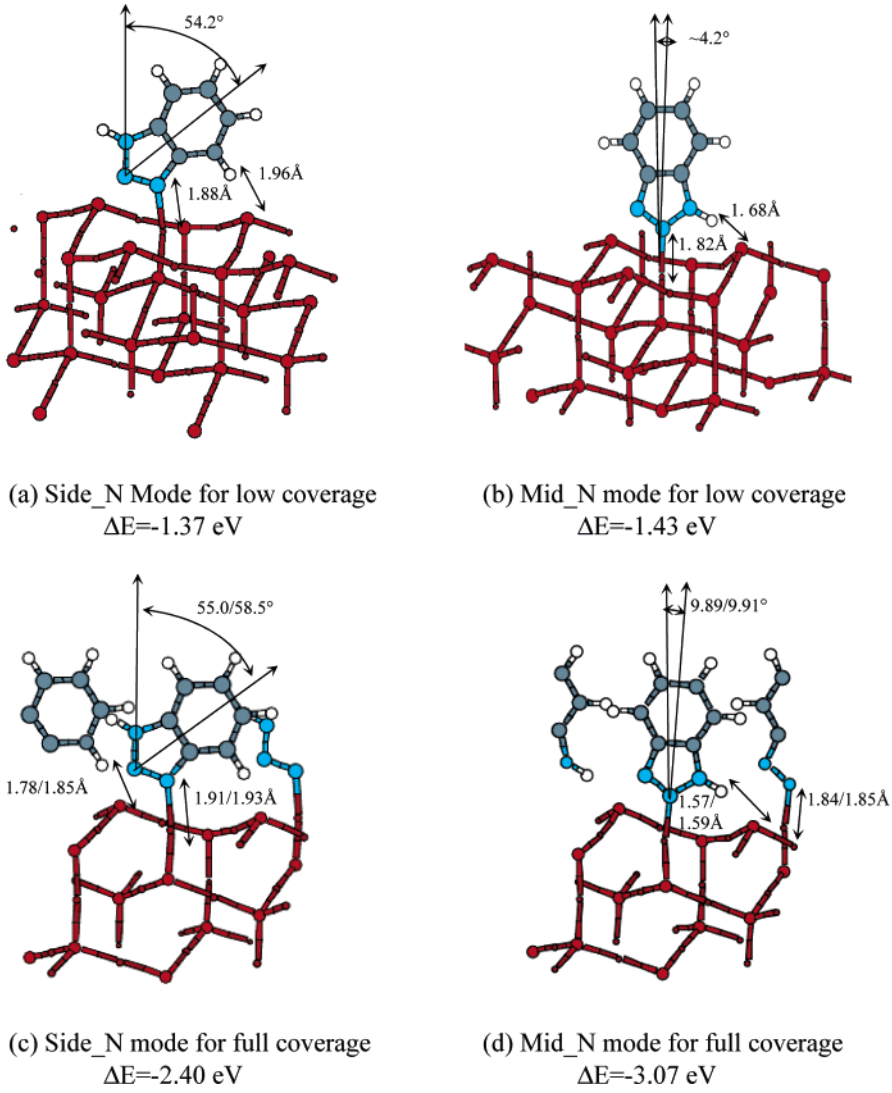

(a) Side_N Mode for low coverage
ΔE=-1.37 eV

(b) Mid_N mode for low coverage
ΔE=-1.43 eV

(c) Side_N mode for full coverage
ΔE=-2.40 eV

(d) Mid_N mode for full coverage
ΔE=-3.07 eV

Figure 3. The energy-minimized binding geometries and energies for BTAH adsorptions on $Cu_2O(111)$.

Negative ΔE represents an energy-favored adsorption. The obtained energy-minimized structures and binding energies are shown in Figure 3.

We notice that in both the Side_N and the Mid_N mode, BTAH can firmly bond on the $Cu_2O(111)$ and reduce the whole system's total energy by 1.2−1.5 eV, therefore the two adsorption structures may coexist. However, the ΔE comparison contradicts the usual assumption based on the Hirshfeld charge analysis only, in which N_3 possesses more charge than N_2, and should more actively interact with $Cu(L_s^a)$ sites in the Side_N mode. In fact, four factors need to be considered for the chemisorption of BTAH/$Cu_2O(111)$: electrostatic (ion-dipole) interactions, σ donation from lone pairs to empty orbitals of Cu(I), π back-donation from filled Cu(I) d-orbital to molecule π^* orbitals, and hydrogen bonding. To explain the controversy, we resort to the binding coordination and the associated hydrogen bond: (1) $Cu_2O(111)$ is an open surface where the surface cations are less coordinated and more exposed, but due to the orientation constraint of the BTAH molecule, only the Mid_N mode allows a strong ion−dipole interaction. A strong ion−dipole interaction enables the molecule to approach closer to the surface Lewis acid−base pairs, increasing orbital overlaps for σ donation, π back-donation, and hydrogen bond formation. (2) A linear dependence between the electrostatic potential at the hydrogen atom and the energy of hydrogen bond formation has been found recently by Dimitrova et al.[33] In a BTAH molecule, the N_1-H_{10} with a charge distribution of of −0.034 and +0.157 e and distance (d) of 1.01 Å definitely experiences a much stronger electrostatic potential at the hydrogen atom than the C_5-H_{14} (−0.034, +0.050 e; d = 1.09 Å) does, and the $N-H\cdots O(L_s^b)$ is thus much stronger. On the basis of many previous ab initio[34,35] and experimental[36] studies, it is not unreasonable to estimate $N-H\cdots O(L_s^b)$ could be 3−4 times stronger than $C-H\cdots O(L_s^b)$, which can cause a 0.2−0.3 eV difference of adsorption energies. This strength difference is also reflected in the unusually short bond length of $N-H\cdots O(L_s^b)$ [L_{N-H} = 1.08 Å, $L_{H\cdots O}$ = 1.58 Å, $L_{N\cdots O}$ = 2.65Å, ∠N−H···O = 169°] compared with the longer $C-H\cdots O(L_s^b)$ [L_{C-H} = 1.10 Å, $L_{H\cdots O}$ = 1.85Å, $L_{C\cdots O}$ = 2.90 Å, ∠N−H···O = 167°].

4.2. Electronic Properties: Electron Localization Function and Density of States. The ELF (Electron Localization Function) was initially proposed by Becke and Edgecombe[39] to measure electron pairing by defining

$$\mathrm{ELF} = \frac{1}{1 + (D(r)/D_h(r))^2} \qquad (2)$$

The term $D(r)/D_h(r)$ normalizes the same-spin probability by the uniform-density electron gas as reference, and thus ELF is a dimensionless localization index restricted to the range of [0,1]. A high ELF value stands for a low probability of finding a

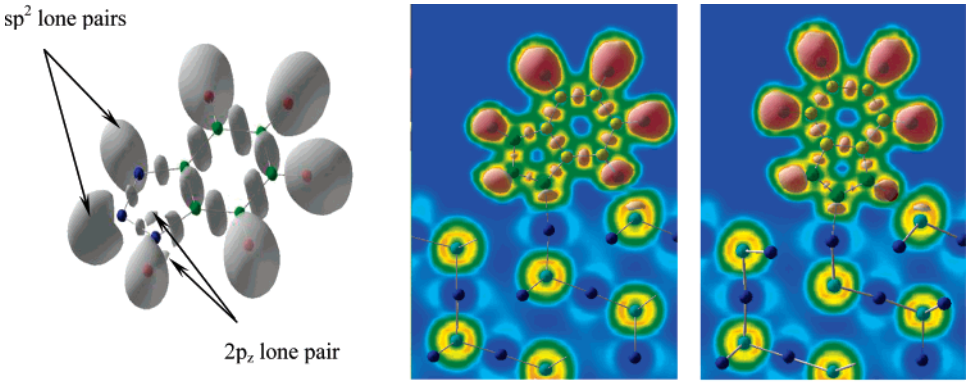

Figure 4. ELF = 0.85 isosurface for an isolated BTAH (a) and an adsorbed BTAH in both adsorption modes (b, c).

second electron with the same pine in the neighboring region of the reference electron, i.e. the reference electron is highly localized. Figure 4 shows the ELF = 0.85 isosurface for an isolated BTAH and an adsorbed BTAH in both modes. In Figure 4a, a spherical basin is visible for each proton. Out of the five valance electrons of N_1, three are involved in σ-bonding by sp^2 hybridization, and two form a $2p_z$ lone pair. In either N_2 or N_3, two valance electrons are involved in σ-bonding, two form a sp^2 lone pair, leaving one p electron in the triazole's π-ring. By comparing (b) and (c) with (a), one can see that after adsorption, the large bean-shaped sp^2 lone-pair basin of N_2 or N_3 reduces to be a small lobe-shaped one, and that the spherical basin of the C−H or N−H proton distorts due to the formation of the hydrogen bond with the surface oxygen anion. ELF plots support the concept that BTAH is chemisorbed on the Cu_2O-(111) surface at the $Cu(L_s^a)$ site through the molecular lone pairs, which is further stabilized by the hydrogen bond forming with the $O(L_s^b)$ site.

Direct electronic evidence of chemical adsorption is present in Figure 5, which shows the projected electronic density of states (DOS) on surface copper and the gas-phase molecule for both modes. The interaction between the molecule and the substrate is very complicated. The BTAH MO's of interest can be divided into two groups: nine π orbitals perpendicular to the molecule plane and two lone-pair orbitals. The most interesting MO's are 3π (composed of 25% N_1-, 28% N_3-, 12% C_4-, 10% C_5-, 7% C_8-, 10% C_9-p_y's), 4π (of 19% N_2-, 22% C_4-, 11% C_6-, 25% C_7-, 14% C_9-p_y's), 5π (of 17% N_1-, 11% N_3-, 21% C_5-, 17% C_6-, 24% C_8-p_y's), 16σ (bonding sp^2 lone pairs, composed of 54% N_2-, 22% N_3-sp^2), 17σ (antibonding sp^2 lone pairs, composed of 23% N_2-, 55% N_3-sp^2), and $6\pi^*$ (of 26% N_2-, 12% N_3-, 19% C_5-, 13% C_7-, 19% C_8-p_y's) as labeled in Figure 5 (the $x-y-z$ coordination here is defined globally for the molecule and the surface, and therefore all the moleculae's π-bondings are formed by p_y's). It can be seen from Figure 5a that Cu-$3d_{z^2}$ hybridizes with the 4s and $4p_z$ states before adsorption, splitting into hybrid bonding and antibonding contributions to DOS. This $d_{z^2}sp_z$ hybridization can explain the unusual linear coordination of O−Cu−O and the remarkably short Cu−Cu distance in Cu_2O bulk.[38,39] In (b) the $d_{z^2}sp_z$ hybrid states further split after reacting with the molecule. The $d_{z^2}sp_z$ hybrid interaction with the 16σ lone pair results in bonding states at −8.3 eV and antibonding states mostly spread above 2 eV. The accumulation of Cu-s, -p_z, and -d_{z^2} states suggests a charge donation from the molecule to the surface.

The σ-donation is fairly strong so that the 16σ level is stabilized upon chemisorption by 4.2 eV. The 5π HOMO has no AO contribution from N_2, and experiences little interaction with the substrate. The d_{xy} and the $d_{x^2-y^2}$ orbital remains almost intact due to its geometry and symmetry, but the d_{yz} states can interact with the 4π and the $6\pi^*$ MO's. The d-π states between −2 to 0 eV have contributions from both the antibonding d-4π and bonding d-$6\pi^*$ orbitals. Since the 4π orbital is completely filled, the 4π-d_{yz} interaction does not contribute to the bonding. The interaction with the 4π orbital, located at the lower end of the metal d_{yz} states, tends to shift the dyz states to higher energy, whereas interaction with the $6\pi^*$ orbital pushes them to lower energy. Both effects cannot be strong since the occupation of the d-π states is low, and as a result the d_{yz} states experience a small downshift only. In the Side_N mode, the bonding mechanism is similar, except that the σ-donation now involves the 17σ and the π back-donation involves the 3π and 5π MO's. The 17σ-$d_{z^2}sp_z$ interaction stabilizes the 17σ level by 5 eV, indicating a stronger σ-donation in the Side_N mode. Correspondently, a remarkable increase of the intensities of Cu-s, -p_z, and -d_{z^2} states is visible in Figure 5c. This agrees very well with the Hirshfeld-charge based prediction by which N_3 should more actively interact with $Cu(L_s^a)$ sites than N_2. The d-$6\pi^*$ orbital interaction is weaker, however, and the antibonding d-$6\pi^*$ hybrid orbital moves to lower energies. Just like the 4π-d_{yz} interaction in the Mid_N mode, the $3\pi/5\pi$-d_{yz} interaction does not contribute to the bonding. One can conclude that for the chemisorption mechanism, the ion−dipole interaction brings the molecule close to the binding site, the donation from the molecular lone-pair orbital to the substrate tends to drive the molecule toward the surface $Cu(L_s^a)$ site to form a chemsorption through the Side_N atom (N_3), whereas the hydrogen bond and the π back-donation from the substrate to the $6\pi^*$ orbital favors a chemsorption through the Mid_N atom (N_2).

4.3. External Stretching Frequency. In this section, we consider only the external stretching for both adsorption structures although the wagging vibration is also expected. For both adsorption modes, the stretching frequencies are derived by using a grid of 11 displacements of the bonded N atom separated by 0.02 Å each vs total energies. The anharmonic correction is negligible ($\sim$1 cm^{-1}).

We employ the well-known Morse potential to describe long-range behavior

$$E = A(1 - e^{-\alpha}(r - r_0))^2 + B \quad (3)$$

To extract A, B, α, and r_o, a forth-order polynomial approximation of Morse potential is used to fit the calculated energies E with small displacements from the equilibrium distance r_o.

$$E = B + A\alpha^2(r - r_o)^2 - A\alpha^3(r - r_o)^3 + \frac{A}{4}\alpha^4(r - r_o)^4 \quad (4)$$

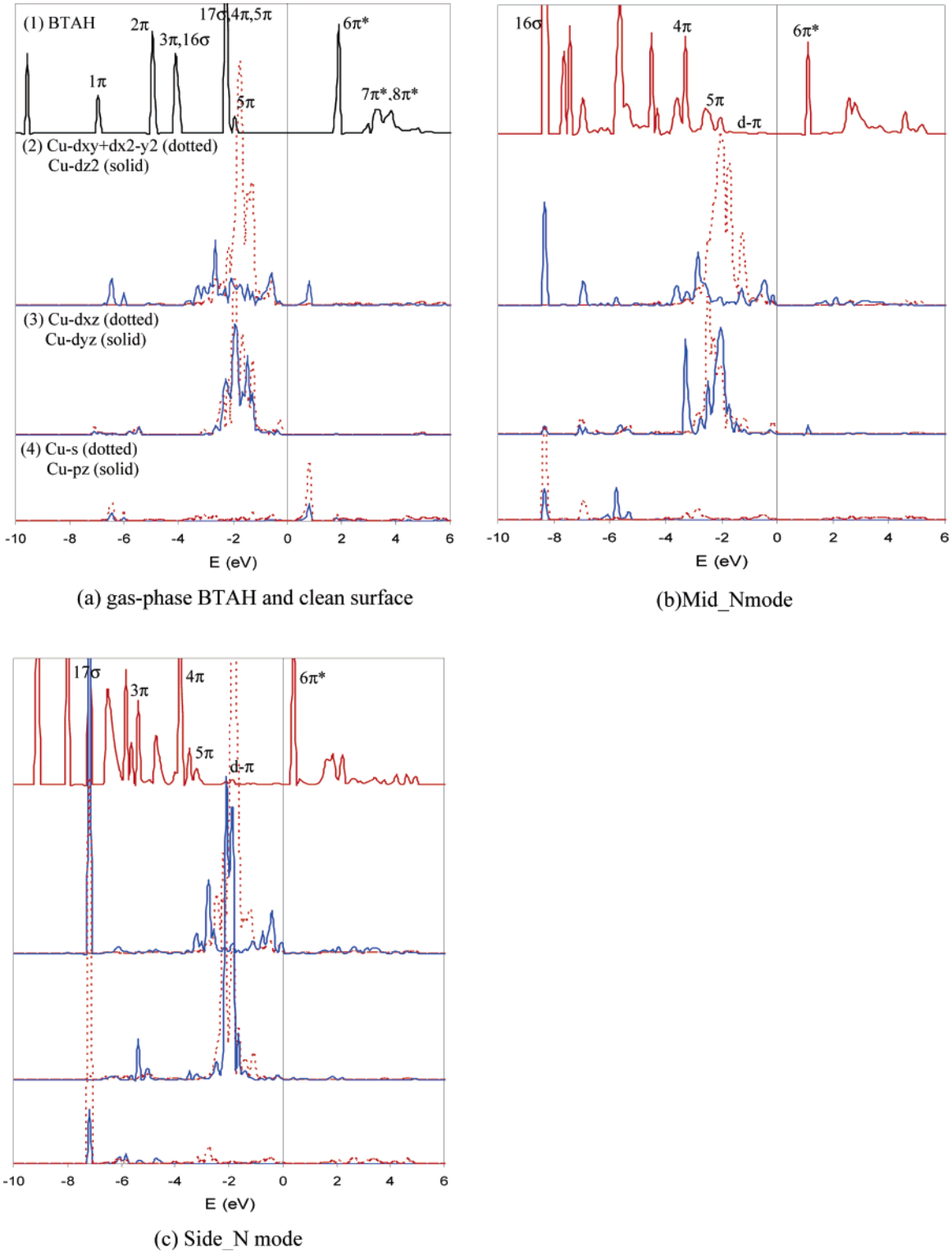

Figure 5. Projected electronic density of states on the molecule and the surface copper. The zero energy corresponds to the Fermi level. The zero energy for the gas-phase molecule corresponds to the middle energy between HOMO and LUMO.

The external stretching frequency, ν_e^s, and anharmonicity-corrected frequency, ν_e^{s-a} (if applied), thus can be obtained by

$$A\alpha^2 = \frac{1}{2}\mu(2\pi\nu_e^s)^2 \tag{5}$$

$$\nu_e^{s-a} = \nu_e^s\left[1 - 2\frac{\alpha^2\hbar}{2\mu(2\pi\nu_e^s)}\right] \tag{6}$$

where μ is the reduced mass of the system, and A is the well-depth; D_e = dissociation energy D_o + zero energy ($^1/_2h\nu_e^s$). The calculated r_e, D_o, K_e, and ν_e^s values are shown in Table 2.

It would be interesting to compare the Morse-potential fitting results in Table 2 with the data in Figure 3. The obtained dissociation energies in Table 2, D_o(N−Cu(I)), are only 4%/0.6% different from the adsorption energies obtained in Figure 3c,d for the Side_N/Mid_N mode, respectively. The equilibrium distances are a little shorter than those obtained from relaxation calculations, which is reasonable considering the contribution of the hydrogen bond to the adsorption. In reality,

TABLE 2: Calculated Equilibrium Distance, r_e, Dissociation Energy, D_o, Force Constant, K_e, and the Stretching Frequency, ν_e^s, for Both Adsorption Modes

adsorption mode	r_e (Å)	D_o (eV)	K_e (kg/s^2)	ν_e^s (cm^{-1})
Side_N	1.89	1.25	1020	381
Mid_N	1.83	1.55	1228	429

the BTAH molecule stretches under the combined effect of a hydrogen bond and a N−Cu(L_s^a) bond. As a consequence, the equilibrium distances determined by Morse-potential fitting are less reliable than those obtained by the energy-minimization calculations. Another DFT calculation for $NH_3/Cu_2O(111)$ reported a harmonic stretching frequency of ∼453 cm^{-1},[40] which is in reasonable agreement with our result for BTAH/Cu_2O-(111). A direct theoretical comparison for BTAH/Cu_2O(111) is still not available. There have been few SERS (Surface Enhanced Roman Spectroscopy) analyses of BTAH on polycrystalline copper or copper oxide electrode: It was reported by Chan et al.[41] for a BTAH/copper-electrode system that a medium-strong peak at ∼240 cm^{-1} measured in a pH 2 solution at −0.7 V (vs SCE) could be assigned to the Cu−N bond that is connected through the nitrogen lone pair. Since the formation of bulk-phase Cu(I)BTA complex is not anticipated under this potential and pH value by the Pourbaix diagram,[14] we should ascribe the ∼240-cm^{-1} peak to the stretching vibration of a monolayer (or less) BTAH on a pure Cu surface. This can be further correlated with the weak binding strength of ∼0.43 eV by our previous calculation[13] if (111) surfaces dominate on the copper electrode. To the best of our knowledge, the only vibrational analysis of BTAH/copper oxide was done by Xu et al.[16] by means of SERS. For BTAH on an oxidized copper electrode, the bands of oxides (Cu_2O) in the 520−590-cm^{-1} region were wide and strong in intensity, making the Raman signals of the adsorbed BTAH rather weak. Even worse, the benzene ring torsion of BTAH unfortunately occurs at 434 cm^{-1},[42] and could shift to 410 cm^{-1} after being bonded to Cu_2O. This band is so close to our calculated frequency values that υ_e(N−Cu(I)) possibly overlaps with the benzene ring torsion band of BTAH, making it hard to distinguish. Furthermore, using our calculated υ_e(N−Cu(I)) for BTAH/Cu_2O, and knowing that D_e is proportional to υ_e^2 (eq 5), then we can estimate the υ_e(N−Cu^0) for BTAH/Cu by $\upsilon_e(N-Cu^0) \approx \upsilon_e(N-Cu(I)) \times (D_e(N-Cu^0)/D_e(N-Cu(I)))^{1/2}$. Using ν_e^s(N−Cu(I)) of the Mid_N mode, $\upsilon_e(N-Cu^0) = 429 \times (0.43/1.55)^{1/2} = 226$ cm^{-1}, and using ν_e^s(N−Cu(I)) of the Side_N mode, $\upsilon_e(N-Cu^0) = 381 \times (0.43/1.25)^{1/2} = 223.4$ cm^{-1}. Both are in good agreement with the experimental value of 240 cm^{-1}.[41]

5. Conclusion

Since the $Cu_2O(111)$ surface has Lewis acid−base site pairs, we propose two possible bound structures for the BTAH/Cu_2O-(111) system: Mid_N mode and Side_N mode. We have calculated the adsorption geometry and binding energy for both modes by using DFT GGA calculations. It is found that BTAH can be firmly chemisorbed onto the surface in both cases and the chemisorption is due to the combined effect of a chemical bond with surface copper cation through nitrogen sp^2 lone pairs and a hydrogen bond with a surface oxygen anion through C−H or N−H protons. The total energy calculations show that the chemisorption in the Mid_N mode is stronger than that in the Side-N mode, which conflicts with the usual assumption based on Hirshfeld charge analysis. The stronger ion−dipole interactions, the more efficient π back-donation, and the stronger hydrogen bond in the Mid_N mode should be responsible for this discrepancy. Although some of the electron states of the molecule−substrate system exhibit significant hybridization before adsorption and rehybridization after adsorption, a molecular-orbital based analysis is still essential for a simple understanding of the chemisorption mechanism: the σ-donation from the lone-pair molecular orbital to the Cu-$d_{z^2}sp_z$ hybrid orbital, combined with the hydrogen bond and the π back-donation from the Cu-d_{yz} to the $6\pi^*$ LUMO. To predict the external stretching frequency of the chemisorption, vibration frequency calculations have been carried out. No direct theoretical or experimental comparison with our calculation is available now, but our computed υ_e(N−Cu(I)) for BTAH/Cu_2O(111) is reasonably close to another DFT result for NH_3/Cu_2O(111). The external stretching υ_e(N−Cu(I)) of BTAH/Cu_2O(111) could overlap with the benzene ring torsion band of BTAH. An estimate for the BTAH/Cu vibrational frequency (226 cm^{-1} by $\nu_e^s(N-Cu(I))_{Mid\_N}$ or 223.4 cm^{-1} by $\nu_e^s(N-Cu(I))_{Side\_N}$) agrees well with an experimentally observed Raman peak of 240 cm^{-1}.

Acknowledgment. This paper is based upon work supported by the National Science Foundation under Grant No. NSF-DMI 9974381. Any opinions, findings, conclusions or recommendations expressed in this paper are those of the authors. The authors wish to thanks Dr. Georg Kresse and the VASP group of the University of Vienna, Austria, for their technical assistance with VASP code. Y. Jiang also wishes to thank Dr. Timothy Steimle, Newton Ooi, and Jun Zhong (ASU) for helpful discussions and Dr. Evgueni Chagarov for maintaining our 4-node Alpha cluster. The computational resources of the National Computational Science Alliance (NCSA) at UIUC are also gratefully acknowledged.

References and Notes

(1) Singh, R. K.; Lee, S.-M.; Choi, K.-S.; Basim, G. B.; Choi, W.; Chen. Z.; Moudgil, B. M. *MRS Bull.* **2002**, *27*, 752.
(2) Shon-Roy, L. *Solid State Technol.* **2000**, *43*, 67.
(3) Singh, R. K.; Bajaj, R.; Moinpour, M.; Meuris, M. *Mater. Res. Soc. Symp. Proc.* **2001**, 613.
(4) British Patent 625,339, December 1947.
(5) Steigerwald, J. M.; Murarka, S. P.; Gutmann, R. J.; Duquette D. J. *Mater. Chem. Phys.* **1995**, *41*, 217.
(6) Stavreva, Z.; Zeidler, D.; Plotner, M.; Drescher, K. *Appl. Surf. Sci.* **1995**, *91*, 192.
(7) Gutmann, R. J.; Steigerwald, J. M.; You, L.; Price, D. T.; Neirynck J.; Neirynck, D. J.; Murarka, S. P. *Thin Solid Film* **1995**, *270*, 596.
(8) Carpio R.; Farkas, J.; Jairath, R. *Thin Solid Film* **1995**, *266*, 238.
(9) Luo, Q.; Compbell, D. R.; Babu, S. V. *Langmuir* **1996**, *12*, 3563.
(10) Len, V. S. C.; MeNeill, D. W.; Gamble, H. S. *Mater. Res. Soc. Symp. Proc.* **2000**, *613*, Spring, E 7.4.1.
(11) Nilsson, J.-O.; Tornkvist, C.; Liedberg, B. *Appl. Surf. Sci.* **1989**, *37*, 306.
(12) Cohen, S. L.; Brusic, V. A.; Kaufman, F. B.; Frankel. G. S.; Motakef, S.; Rush, B. M. *J. Vac. Sci. Technol. A* **1990**, *8*, 2417.
(13) Jiang, Y.; Adams, J. B. *Surf. Sci.* **2003**, *529*, 428.
(14) Tromans, D. *J. Electrochem. Soc.* **1998**, *145*, L42.
(15) Mansfeld, F.; Smith, T. *Corrosion* **1973**, *29*, 105.
(16) Xue, G.; Ding, J.; Lu, P.; Dong, J. *J. Phys. Chem.* **1991**, *95*, 7380.
(17) Chu, Y. S.; Robinson, I. K.; Gewirth, A. A. *J. Chem. Phys.* **1999**, *110*, 5952.
(18) *VASP Guide*; http://cms.mpi.univie.ac.at/vasp/.
(19) Perdew, J. P.; Wang, Y. *Phys. Rev. B* **1992**, *45*, 13244.
(20) Kresse, G. *VASP Training Notes*; August, 1999.
(21) *ADF Users Guide*; SCM/Vrije Universiteit: Amsterdam, The Netherlands, 2002.
(22) Restori, R.; Schwarzenbach, D. *Acta Crystallogr. B* **1986**, *42*, 201.
(23) Ruiz, E.; Alvarez, S.; Alemany, P.; Evarestov, R. A. *Phys. Rev. B* **1997**, *56*, 7189.
(24) Beg, M. M.; Shapiro, S. M. *Phys. Rev. B* **1976**, *13*, 1728.
(25) Hallberg, J.; Hanson, R. C. *Phys. Status Solid B* **1970**, *42*, 305.
(26) Henrich, V. E.; Cox, P. A. *The Surface Science of Metal Oxides*; Cambridge University Press: Cambridge, UK, 1996; Chapter 2.
(27) Te Velde, G. *Numerical integration and other methodological aspects of bandstructure calculations in Chemistry*; Vrije Universiteit: Amsterdam, The Netherlands, 1990.
(28) Bickelhaupt, F. M.; et al. *Organometallics* **1996**, *15*, 2923.

(29) Fonseca Guerra, C.; et al. *Chem. Eur. J.* **1999**, *5*, 3581.
(30) Hirshfeld, F. L. *Theor. Chim. Acta* **1977**, *44*, 129.
(31) Wiberg, K. B.; Rablen, P. R. *J. Comput. Chem.* **1993**, *14*, 1504.
(32) Iglesla, E.; Barton, D. G.; Biscardi, J. A.; Gines, M. J. L.; Soled, S. L. *Catal. Today* **1997**, *38*, 339.
(33) Dimitrova, V.; Ilieva, S.; Galabov, B., Jr. *Mol. Struct.* (*THEOCHEM*) **2003**, *637*, 73.
(34) Schneider, S.; Kar, T.; Gu, Y. *J. Biol. Chem.* **2001**, *276*, 9832.
(35) Marten, B.; Kim, K.; Cortis, C.; Friesner, R. A. *J. Phys. Chem.* **1996**, *100*, 11775.
(36) Zwier, T. S. *Annu. Rev. Phys. Chem.* **1996**, *47*, 205.
(37) Laskowski, R.; Blaha, P.; Schwarz, K. *Phys. Rev. B* **2003**, *67*, 075102.
(38) Mertz, K. M.; Hoffman, R. *Inorg. Chem.* **1988**, *27*, 2120.
(39) Becke, D.; Edgecombe, K. E. *J. Chem. Phys.* **1990**, *92*, 5397.
(40) Casarin, M.; Maccato, C.; Vittadini, A. *Chem. Phys. Lett.* **1999**, *300*, 403.
(41) Chan, H. Y. H.; Weaver, M. J. *Langmuir* **1999**, *15*, 3348.
(42) Bigotto, A.; Pandey, A. N.; Zerbo, C. *Spectroc. Lett.* **1996**, *29*, 511.